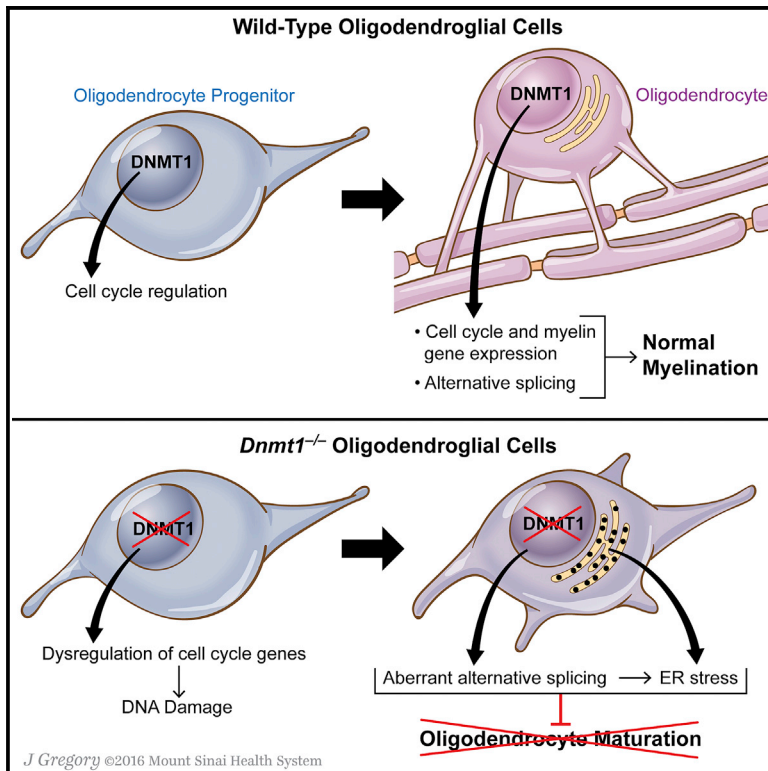


Functional Characterization of DNA Methylation in the Oligodendrocyte Lineage

Graphical Abstract



Authors

Sarah Moyon, Jimmy L. Huynh, Dipankar Dutta, ..., Jun Zhu, Jeffrey L. Dupree, Patrizia Casaccia

Correspondence

patrizia.casaccia@mssm.edu

In Brief

Moyon et al. combine high-resolution methylomics, RNA sequencing, and analysis of multiple transgenic lines to define a critical role for DNA methylation in developmental myelination. Ablation of *Dnmt1* decreases proliferation yet minimally impacts progenitors while impairing the late stages of differentiation, which require alternative splicing.

Highlights

- Oligodendrocyte-lineage-specific analysis of DNA methylome and transcriptome
- No fate switch induced by *Dnmt1* ablation in early oligodendrocyte progenitors
- DNMT1-dependent regulation of differentiation-specific alternative splicing events
- Impaired myelination in *Dnmt1* mutants characterized by aberrant ER stress response

Accession Numbers

GSE66047



Functional Characterization of DNA Methylation in the Oligodendrocyte Lineage

Sarah Moyon,^{1,12} Jimmy L. Huynh,^{1,2,12} Dipankar Dutta,³ Fan Zhang,¹ Dan Ma,^{5,6} Seungyeul Yoo,² Rebecca Lawrence,¹ Michael Wegner,⁷ Gareth R. John,^{3,4} Ben Emery,⁸ Catherine Lubetzki,⁹ Robin J.M. Franklin,^{5,6} Guoping Fan,¹⁰ Jun Zhu,² Jeffrey L. Dupree,¹¹ and Patrizia Casaccia^{1,2,3,4,*}

¹Department of Neuroscience

²Department of Genetics and Genomic Sciences

³Department of Neurology

⁴Corinne Goldsmith Dickinson Center for Multiple Sclerosis
Icahn School of Medicine at Mount Sinai, New York, NY 10029, USA

⁵Wellcome Trust-Medical Research Council Cambridge Stem Cell Institute

⁶Department of Clinical Neurosciences

University of Cambridge, Cambridge CB2 0AH, UK

⁷Institut für Biochemie, Universität Erlangen-Nürnberg, Fahrstrasse 17, 91054 Erlangen, Germany

⁸Jungers Center for Neurosciences Research and Department of Neurology, Oregon Health and Science University, Portland, OR 97239, USA

⁹Sorbonne Universités UPMC Université, Paris 06, UMR_S 1127, ICM-GHU Pitié-Salpêtrière, 75013 Paris, France

¹⁰Department of Human Genetics, David Geffen School of Medicine, University of California, Los Angeles, Los Angeles, CA 90095, USA

¹¹Department of Anatomy and Neurobiology, Virginia Commonwealth University, Richmond, VA 23298, USA

¹²Co-first author

*Correspondence: patrizia.casaccia@mssm.edu

<http://dx.doi.org/10.1016/j.celrep.2016.03.060>

SUMMARY

Oligodendrocytes derive from progenitors (OPCs) through the interplay of epigenomic and transcriptional events. By integrating high-resolution methylomics, RNA-sequencing, and multiple transgenic lines, this study defines the role of DNMT1 in developmental myelination. We detected hypermethylation of genes related to cell cycle and neurogenesis during differentiation of OPCs, yet genetic ablation of *Dnmt1* resulted in inefficient OPC expansion and severe hypomyelination associated with ataxia and tremors in mice. This phenotype was not caused by lineage switch or massive apoptosis but was characterized by a profound defect of differentiation associated with changes in exon-skipping and intron-retention splicing events and by the activation of an endoplasmic reticulum stress response. Therefore, loss of *Dnmt1* in OPCs is not sufficient to induce a lineage switch but acts as an important determinant of the coordination between RNA splicing and protein synthesis necessary for myelin formation.

INTRODUCTION

Brain development requires the integration of cell-lineage selection and cell number regulation. This is achieved by coordinating cell proliferation with lineage identity. DNA methylation is a well-recognized epigenetic modification that is carefully

regulated during cell division and guarantees faithful transmission of information to the daughter cells. This enzymatic activity is modulated by three proteins: DNMT1 (*maintenance* DNA methyltransferase, commonly associated with faithful transmission of genomic information from mother to daughter cells during cell division), DNMT3A, and DNMT3B (*de novo* methyltransferases methylating specific cytosines during development). The activity of these enzymes in the brain is higher than in any other adult tissue (Ono et al., 1993; Tawa et al., 1990), highlighting the importance of DNMTs in neural development (Lister et al., 2013; Smith and Meissner, 2013). This study addresses the role of DNA methylation in developmental myelination.

Genetic loss of *Dnmt1* is lethal in mammals (Li et al., 1992) and zebrafish (Jacob et al., 2015), because rapidly proliferating cells need to retain a stable epigenetic signature and are eliminated by apoptosis if compromised (Jackson-Grusby et al., 2001; Unterberger et al., 2006). An example is the apoptotic elimination of neural stem cells and mitotic neuroblasts lacking *Dnmt1* (Fan et al., 2001; Hutnick et al., 2009; Milutinovic et al., 2003). In contrast, inhibiting DNA methylation in astrocytes or Schwann cells is associated with precocious onset of differentiation, due to the unmasking of critical transcriptional regulatory sites in differentiation genes (Fan et al., 2005; Takizawa et al., 2001; Varela-Rey et al., 2014). In this study, we show that ablation of *Dnmt1* in the oligodendrocyte (OL) lineage does not result in apoptosis or precocious myelination but causes the growth arrest of OL progenitors (OPCs) and a severely disrupted pattern of alternative splicing with the activation of an endoplasmic reticulum (ER) stress response, which precludes differentiation and results in severe and clinically symptomatic hypomyelination.

RESULTS

Dynamic DNA Methylation and DNA Methyltransferase Expression during OL Differentiation

DNA methylation in proliferating progenitors has been shown to prevent untimely differentiation and to guarantee faithful transmission of genomic information from mother to daughter cells during replication (Fan et al., 2005; Probst et al., 2009; Sen et al., 2010; Varela-Rey et al., 2014). To begin characterizing the role of DNA methylation in OL-lineage cells, we quantified 5-methylcytosine (5-mC) in developing white matter tracts during embryonic and postnatal development. Quantification of the percentage of OLIG2+ OPCs expressing 5-mC (Figure 1A) revealed a greater proportion of highly methylated cells at late developmental time points (Figure 1B). A similar pattern was detected in cultured OPCs during differentiation into OLs (Figures 1C and 1D). To further understand the role of DNA methylation in OPCs, we also evaluated the transcript (Figures 1E and 1F) and protein (Figure 1G) levels of the maintenance DNA methyltransferase *Dnmt1* and the de novo methyltransferases *Dnmt3a* and *Dnmt3b* at two stages of development. While *Dnmt1* levels decreased with differentiation, *Dnmt3a* levels did not significantly change, and *Dnmt3b* levels were undetectable at either stage (data not shown).

To generate a genome-wide map of the DNA methylation landscape during the transition from OPC to OL, we used fluorescence-activated cell sorting (FACS) of the brains from transgenic mice expressing GFP driven by OL-lineage-specific promoters at postnatal day (P)2 (*Pdgfra-GFP*) and P18 (*Plp1-GFP*) (Figure 2A). We previously characterized the *Pdgfra-GFP* sorted OPC as expressing progenitor markers (e.g., *Cspg4* and *Pdgfra*) and not expressing myelin genes (e.g., *Mog* and *Mag*), while *Plp1-GFP* sorted OLs were characterized by the expression of differentiation genes and the absence of progenitor markers (Moyon et al., 2015). DNA methylation mapping was performed by enhanced reduced representation bisulfite sequencing (ERRBS), which combined restriction enzyme digestion (i.e., *MspI*) of genomic DNA with bisulfite sequencing and provided single-base resolution and highly quantitative data on the methylation state of cytosines throughout the genome. The mean coverage was 1.47 million individual CpGs in the mouse genome (Table S1), with the majority detected at gene promoters (Figure S1C). Among those, we identified 62,807 differentially methylated CpGs as OPCs differentiated (q value <0.01) with 29,707 hypomethylated and 33,100 hypermethylated CpGs. Regions containing at least two CpGs with a minimum difference of 10% between the two stages of differentiation were classified as differentially methylated regions (DMRs). This revealed the clustering of CpGs into 7,386 DMRs characterizing the differentiation of OPC, with 2,385 hypermethylated regions (with an average methylation difference of $22.2\% \pm 8.5\%$) (Figure S1B). Biological replicates confirmed the reproducibility of the methylation state (Pearson's $r > 0.9$), while comparisons of DMRs in samples obtained at the two developmental time points displayed great disparity (Figure S1A), further supporting the large shift in the DNA methylome during differentiation. To determine the relationship between DNA methylation and transcription, we performed RNA sequencing (RNA-seq) on the same FACS-isolated popula-

tions (Figure 2; Table S2). Separate clustering of the samples isolated at distinct time points and differential expression of stage-specific markers (*Pdgfra*: fold change, -8.2 ; q value = 5.5×10^{-220} ; *Cspg4*: fold change, -7.0 ; q value = 4.5×10^{-169} ; *Plp1*: fold change, 2.3 ; q value = 6.4×10^{-3} ; *Mog*: fold change, 4.9 ; q value = 2.09×10^{-34} ; *Mag*: fold change, 2.4 ; q value = 2.6×10^{-26}) between the two populations confirmed the selectivity of our cell sorting (Figure S2A). The analysis revealed 3,204 upregulated (average fold change = 3.6 ± 1.8) and 3,547 downregulated transcripts (average fold change = 5.6 ± 2.4) during differentiation. Upregulated genes included gene ontology (GO) categories related to lipid metabolism and axon ensheathment, while downregulated categories included cell cycle, cell migration, and neuronal differentiation (Figures S2B and S2C). The overwhelming overlap ($p < 10^{-244}$) of our dataset and the published in vitro RNA-seq study (Zhang et al., 2014) further strengthened the validity of our analysis (Figure S2D).

To characterize the transcriptional consequences of genome-wide distribution of DNA methylation, we overlapped the differential transcript expression with DNA methylation differences at promoters and represented the analysis as quadrant plot, based on statistical power (Figure 2B). The most statistically significant differences (based on number of events and difference at the two developmental stages) were identified in two quadrants (I and IV). The highest significance was detected in quadrant IV ($p = 8.1 \times 10^{-19}$), which defined hypermethylated genes with decreased expression during differentiation and included genes related to neuronal lineage (e.g., *Pax6*, *Plxn2*, *Camk1*, and *Ephb2*) and proliferation (e.g., *Cdc6* and *Meis2*) (Figures 2D and 2F). Quadrant I was also significant ($p = 2.5 \times 10^{-7}$) and included hypomethylated genes with increased expression during differentiation, such as lipid enzymes, myelin components (e.g., *Mog* and *Mag*), and enzymes enriched in the myelin compartment such as carbonic anhydrase II (*Car2*), as well as molecules associated with the differentiated state such as the G-protein-coupled receptor 37 (*Gpr37*) (Figures 2C and 2E). The other two quadrants (hypomethylated genes with decreased expression or hypermethylated genes with increased expression during differentiation) did not reach statistical significance and, therefore, were not pursued any further. Taken together, these data highlight the relevance of DNA methylation in OPCs for silencing genes related to cell proliferation and neuronal lineage.

Ablation of *Dnmt1*, but Not *Dnmt3a*, in OPCs during Development Impairs Differentiation and Results in Widespread Myelination Deficits

To define the functional role of DNA methylation in the OL lineage in vivo, we crossed the *Dnmt1^{fl/fl}* and *Dnmt3a^{fl/fl}* lines with *Olig1-cre* to target embryonic progenitors and with the *Cnp-cre* line to target later stages of OL development. Littermates lacking *cre* expression were used as controls. The cell specificity of gene ablation was confirmed by double immunofluorescence, using antibodies specific for DNMT1 (Figure 3A) or DNMT3A (Figure 3B) and those specific for cell markers. Lack of DNMT1 or DNMT3A immunoreactivity in OLIG2+ cells, but not in glial fibrillary acidic protein (GFAP)-positive (GFAP+) or neuronal-marker (NeuN)-positive (NeuN+) cells, indicated lineage-selective ablation

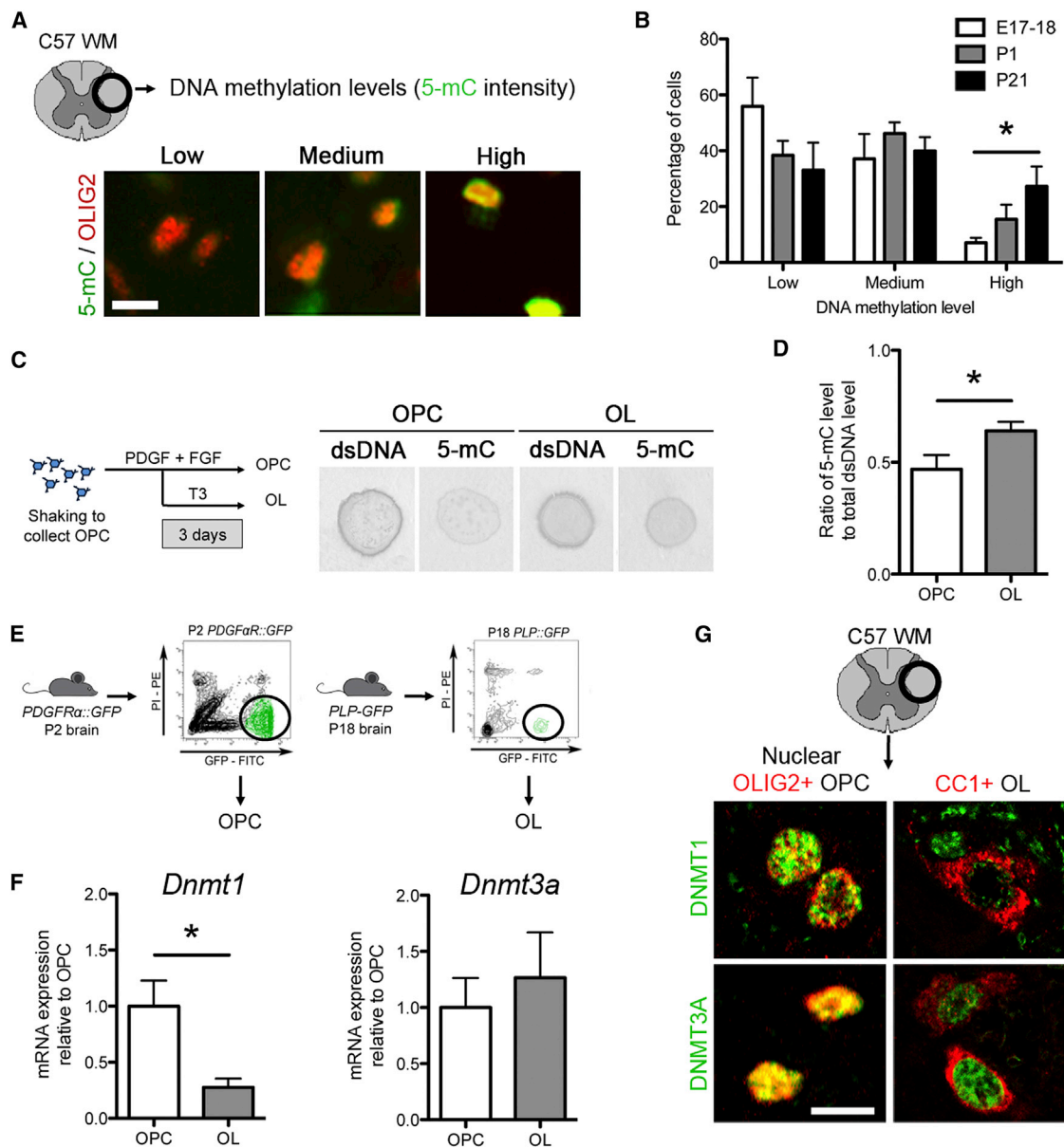


Figure 1. Increased Levels of DNA Methylation and Dynamic Expression of DNA Methyltransferases during OL Development

(A) Immunostaining of DNA methylation using 5-mC antibody (green) and OLIG2 (red) in spinal cord sections revealed the presence of cells with low, medium, and high 5-mC levels of staining intensity.

(B) Quantification of 5-mC immunoreactive OLIG2+ cells in mouse developing spinal cord white matter at E17–E18 (E17-18), P1, and P21.

(C) Left: protocol for culturing proliferating OPCs (PDGF + FGF [fibroblast growth factor]) and inducing differentiation into OLs (T3). Right: dot-blot analysis for 5-mC and dsDNA as control.

(D) Quantification of 5-mC levels relative to total dsDNA in OPCs and OLs.

(E) Scheme of FACS of P2 *PDGFRα::GFP* OPCs and P18 *PLP::GFP* OLs. FITC, fluorescein isothiocyanate.

(F) *Dnmt1* and *Dnmt3a* mRNA levels in sorted OPCs and OLs relative to OPCs.

(G) Representative image of nuclear DNMT1 and DNMT3A (green) immunostaining in OLIG2+ OPCs and CC1+ OLs (red).

Scale bars, 10 μm. Data represent mean ± SEM. **p* < 0.05 (ANOVA and Student's *t* test).

(Figures 3A and 3B). Both *Olig1^{cre/+};Dnmt1^{fl/fl}* and *Olig1^{cre/+};Dnmt3a^{fl/fl}* mice appeared normal at birth; however, by P9, only the *Olig1^{cre/+};Dnmt1^{fl/fl}* mice developed tremors and ataxia (Movie S1), eventually leading to decreased survival by the third postnatal week (Figure 3C). Both *Olig1^{cre/+};Dnmt1^{fl/fl}* and

Cnp^{cre/+};Dnmt1^{fl/fl} mice showed no obvious phenotype (Figure 3C). Consistent with these observations, myelin basic protein (MBP) staining of spinal cord sections at P16 revealed a dramatic hypomyelination only in the *Olig1^{cre/+};Dnmt1^{fl/fl}* mice (Figure 3D). Gross examination of *Olig1^{cre/+};Dnmt1^{fl/fl}* mice at P14 revealed

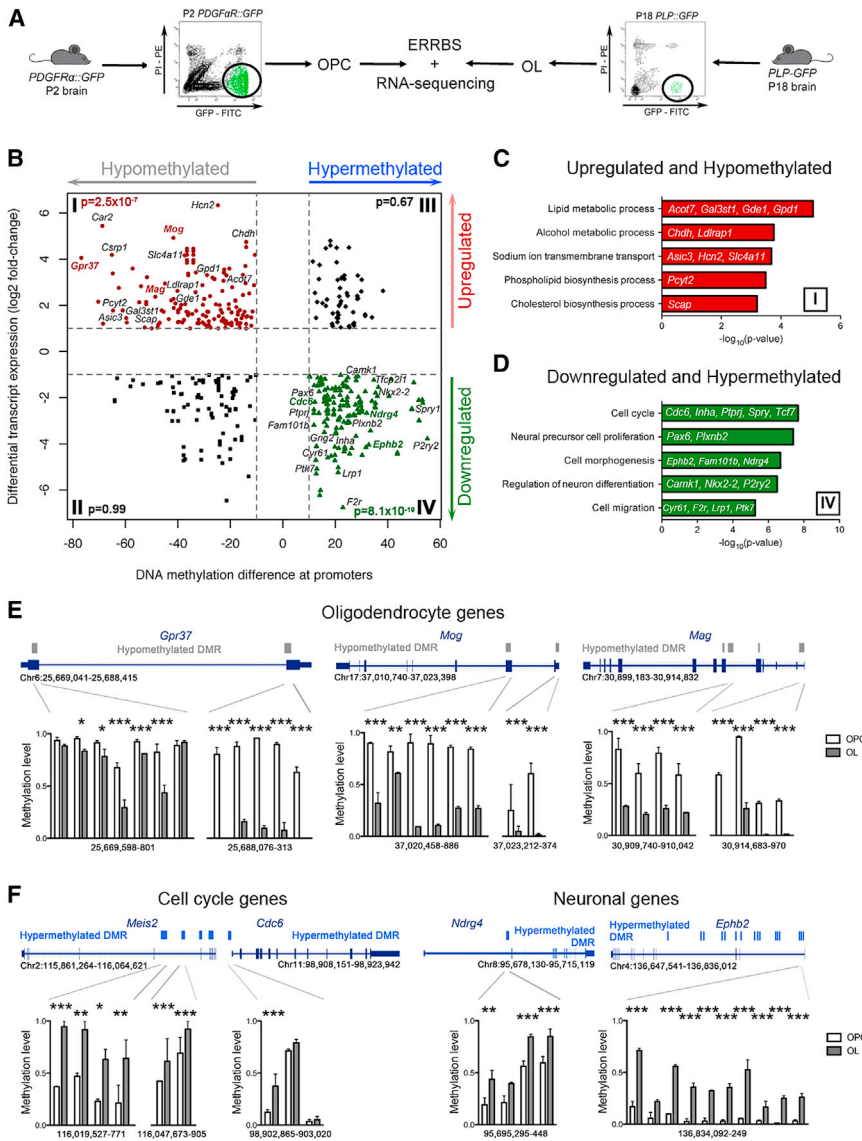


Figure 2. Negative Correlation between DNA Methylation and Transcript Levels in Oligodendroglial-Lineage Cells

(A) Scheme of experimental approach used for RNA-seq and high-resolution methylomics.

(B) Quadrant plot of DMRs at gene promoters and differentially expressed genes (OLS versus OPCs). The x axis refers to DNA methylation differences during differentiation. The y axis indicates log₂ fold change of transcript levels. Horizontal (10% difference) and vertical (2-fold change) dashed lines identify four quadrants: (I) hypomethylated and upregulated genes (red circle), (II) hypomethylated and downregulated (black square), (III) hypermethylated and upregulated (black diamond), and (IV) hypermethylated and downregulated (green triangle). Colored genes in quadrants I and IV are characterized by statistically significant differences in methylation and transcript levels (p value indicated in each quadrant).

(C and D) Top GO categories for upregulated and hypomethylated genes (red; C) and for downregulated and hypermethylated (green; D) genes. (E and F) The bar graphs represent statistically significant DNA methylation levels of individual CpGs (blue boxes over gene structures) in OPCs (white bars) and OLs (gray bars). Note the significantly decreased methylation of CpGs in myelin genes (E) and increased methylation in cell cycle and neuronal genes (F) during differentiation.

Data indicate mean ± SEM. *p < 0.05; **p < 0.01; ***p < 0.005 (false discovery rate).

See also Figures S1 and S2.

only minor differences in body size (Figure 3E) but clear signs of hypomyelination of the spinal cord (see Figure 3F, translucent spinal cord) and brain stem (Figure 3G), which were confirmed by electron microscopy (Figures 3H and S3).

The Hypomyelinated Phenotype Detected in *Dnmt1* Mutants Is Not Attributable to Fate-Lineage Switch

Given the early activity of *Olig1-cre* at the pMN domain (Zhou and Anderson, 2002) and based on the detection of increased methylation and silencing of neuronal lineage-related genes during OPC differentiation, it was important to determine whether the defective myelination phenotype detected in *Olig1^{cre/+}; Dnmt1^{fl/fl}* mice could be attributed to impaired specification. To address this question, we used two approaches. First, we processed spinal cord sections from mutants and control siblings at embryonic day (E)12.5 for immunohistochemistry using antibodies specific for motor neurons (i.e., MNX1), as well as ventral

and the boundaries with the OLIG2+ domain were preserved. We then conducted a fate-mapping analysis crossing the *ROSA26-loxSTOP-lox-TdTomato* reporter line with the *Olig1^{cre/+};Dnmt1^{fl/fl}* or *Olig1^{cre/+};Dnmt1^{+/+}* mice and stained spinal cord sections at P14 with neuronal (NeuN) or astrocytic (GFAP) markers (Figures 4E and 4F). Only very few cells were identified by the reporter expression and staining for NeuN or GFAP, both in controls and mutants (NeuN controls = 2.5% ± 0.3%, mutants = 3.2% ± 1.0%; GFAP controls = 3.0% ± 0.4%, mutants = 3.7% ± 0.6%), suggesting that only very few OPCs differentiated in neurons or astrocytes in the absence of *Dnmt1*.

Dnmt1-Dependent Hypomyelination as a Result of Defective Differentiation

To define the potential cause of the hypomyelinating phenotype, we conducted a quantitative immunohistochemical study of the developing spinal cord from E16.5 to P16 using antibodies

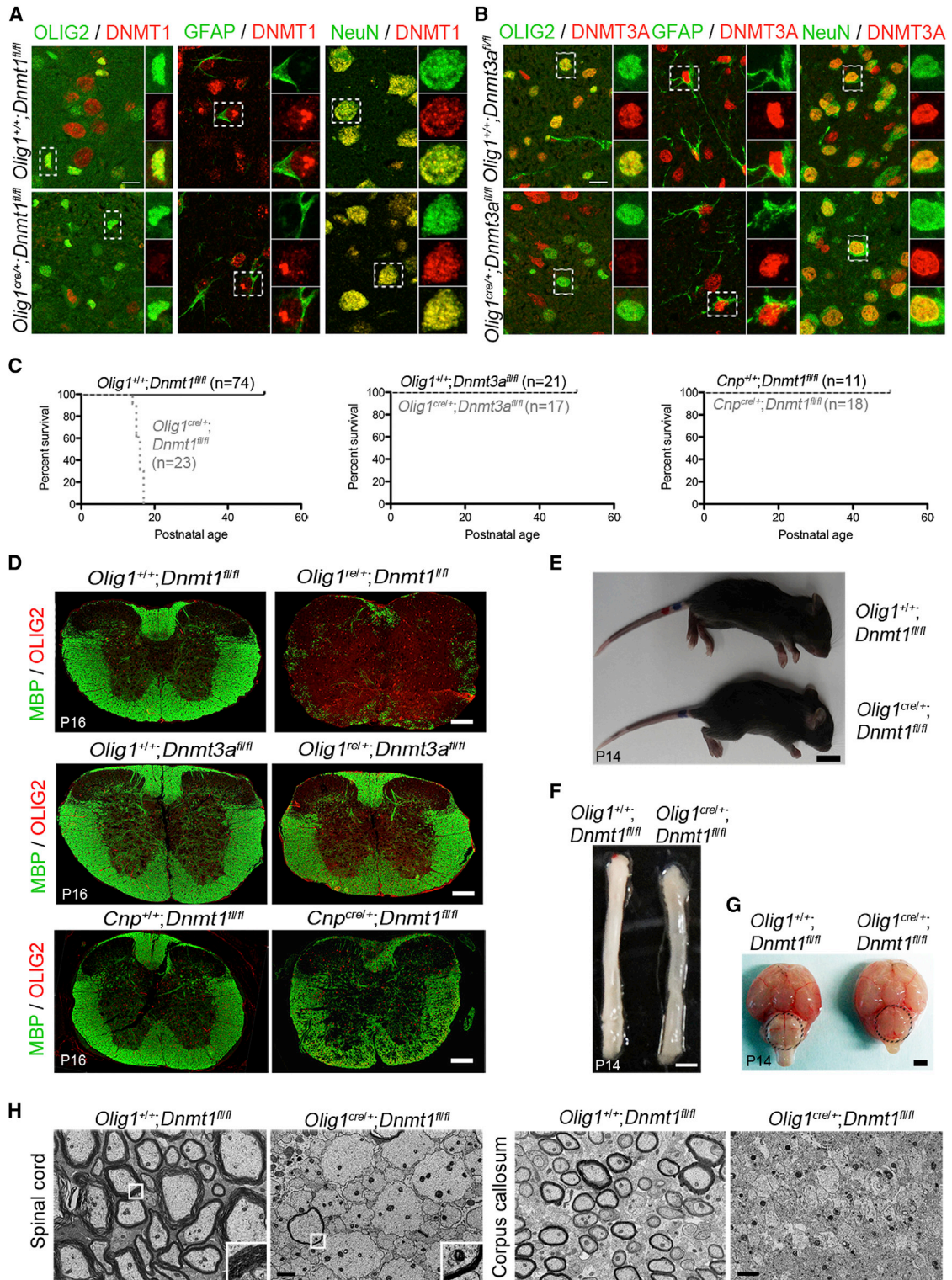


Figure 3. Conditional Ablation of DNA Methyltransferases in OL-Lineage Cells Results in Widespread Hypomyelination in the CNS of *Olig1^{cre/+};Dnmt1^{fl/fl}* Mice

(A and B) Double immunostaining of P16 spinal cord with antibodies for DNMT1 (red; A) or DNMT3A (red; B) and the cell-specific markers (green): OLIG2 for OLs, GFAP for astrocytes, and NeuN for neurons. Note the absence of DNMT1 (A) or DNMT3A (B) in the OL lineage. Scale bar, 10 μ m.

(legend continued on next page)

specific for OLIG2 and platelet-derived growth factor receptor α (PDGFR α) to label OPCs, CC1 to label newly generated OLs, and MBP to label myelinating cells. While a similar number of progenitors was detected in the embryonic spinal cord, a 27% reduction in the number of OPCs was detected in the mutant spinal cords (Figure 5A) and brains (Figure S4A), starting from P2. A greater reduction was observed for newly generated OLs (Figures 5B and S4B), and an even more dramatic impairment was detected when quantifying myelinating MBP+ cells (Figures 5C and S4C), which represent a later stage of differentiation. The cell-autonomous nature of this defect was further validated *in vitro*, which revealed defective differentiation of mutant OPCs compared to controls (Figure 5D). Together, these data support the critical importance of DNMT1 in the OL lineage to coordinate the late stages of differentiation into myelin-forming cells.

To begin understanding the mechanisms underlying the very modest decrease in progenitor numbers and the almost complete absence of myelin detected by electron microscopy, we processed spinal cord sections from controls and mutants at multiple developmental time points for TUNEL (data not shown) or for the presence of active cleaved caspase-3. An accurate assessment of apoptotic nuclei is difficult *in vivo*, due to rapid clearance, and despite the detection toward modestly increased apoptosis at P9, the measurable differences did not reach statistical significance (Figure 6A). An alternative explanation for the reduced OPC number was impaired proliferation. Co-labeling of OPCs with antibodies specific for OLIG2 or PDGFR α and markers of proliferation (i.e., Ki67) or of mitotic activity (i.e., phosphorylated histone H3) (Figures 6B and 6D) identified a clear proliferation defect in mutants. This result was cell intrinsic, as it was also detected in cultured OPCs (Figures 6C and 6E). We concluded that the lower number of OPCs in the developing spinal cord of mutant mice compared to that of age-matched controls could, at least in part, be attributed to defective expansion of the progenitor pool in the absence of *Dnmt1*. Since this phenotype was associated with the detection of concurrent hypomethylation and increased transcripts for genes modulating mitosis (e.g., *Meis2* and *Cdc6*), together with those inhibiting the cell cycle (e.g., *Cdkn1a*), and with the downregulation of positive regulators of proliferation (e.g., *Pdgfra*, *Rbl2*, and *Mcm7*) (Figures 6F and 6G), we reasoned that OPCs might have activated strategies to counteract the consequences of *Dnmt1* ablation after escaping apoptosis. The transcriptional changes leading to opposing effects on proliferation suggested the potential activation of a genotoxic response, possibly resulting in growth arrest. This was validated by the detection of phosphorylated H2AX immunoreactivity, a histone mark demarcating regions of chromatin with double-stranded DNA (dsDNA) breaks (Unterberger et al., 2006), both *in vivo* (Figure 6H) and *in vitro* (Figure 6I).

Ablation of *Dnmt1* in OPCs Activates an ER Stress Response at the Late Stage of Differentiation due to Massive Alteration of Alternative Splicing Events

To better define the dramatic hypomyelinating phenotype of mutant mice, we conducted an unbiased transcriptomic analysis of OPCs sorted from P5 *Olig1^{+/+};Dnmt1^{fl/fl};Pdgfra-GFP* and *Olig1^{cre/+};Dnmt1^{fl/fl};Pdgfra-GFP* using RNA-seq (Figure S5A; Table S3). Loss of *Dnmt1* resulted in 994 downregulated and 566 upregulated genes in mutant cells, compared to controls (Tables S4 and S5). Downregulated genes included myelin genes, OL-specific factors, and lipid metabolism enzymes (Figure S3B), which were further validated by qPCR (Figure S3D). Upregulated gene categories included cell division and response to DNA stress (Figures 6G and S3C). Consistent with the detection of normal lineage specification, we did not detect any upregulation of neuronally enriched gene categories. Because OL differentiation is characterized by alternatively spliced events (Kevelam et al., 2015; Nave et al., 1987), we interrogated our RNA-seq dataset in control and mutant cells (Figure 7A). It has been suggested that DNA methylation in specific genomic regions is critical for exon skipping and intron retention splicing events (Gelfman et al., 2013; Yearim et al., 2015). Consistent with these data, we detected severe impairment of exon skipping and intron retention splicing in mutant OPC (*Olig1^{cre/+};Dnmt1^{fl/fl};Pdgfra-GFP*) compared to wild-type (Figure 7B). These events occurred in GO categories identified as: myelination, lipid metabolism and cell cycle (Figure 7C). An example of splicing defects associated with defective DNA methylation is shown for the gene *Mcm7*, a ubiquitously expressed cell cycle gene characterized by intron retention (Figure 7D). Hypermethylated CpGs in wild-type OPC within the spliced regions were associated with intron splicing while hypomethylated CpGs in mutant cells were associated with intron-retention (Figure 7E). Together, these data provided molecular validation of the relationship between aberrant DNA methylation and alternatively spliced defect, as suggested by the RNA-seq analysis.

It is likely that aberrant splicing might change protein conformation (Kevelam et al., 2015; Yura et al., 2006) and lead to the potential accumulation of incorrectly folded proteins inducing ER stress. Consistent with this possibility, we observed dilated ERs in mutant OLs, with characteristic and unique electron-dense inclusions (Figure 7F), suggestive of protein accumulations and activation of ER stress response. This interpretation was further supported by the detection of specific downstream targets of ER response pathways in mutant mice, including *Bip* (downstream of ATF6), *Chop* (downstream of PERK), and spliced *Xbp1* (downstream of the IRE1 pathway) (Figure 7G). The ER stress response was only detected in *Olig1^{cre/+};Dnmt1^{fl/fl}* mice, as ablation of *Dnmt1* at later stages in *Cnp^{cre/+};Dnmt1^{fl/fl}* mice

(C) Kaplan–Meier survival curves for *Olig1^{+/+};Dnmt1^{fl/fl}* and *Olig1^{cre/+};Dnmt1^{fl/fl}* mice, *Olig1^{+/+};Dnmt3a^{fl/fl}* and *Olig1^{cre/+};Dnmt3a^{fl/fl}* mice, and *Cnp^{+/+};Dnmt1^{fl/fl}* and *Cnp^{cre/+};Dnmt1^{fl/fl}* mice.

(D) Representative P16 spinal cord sections of *Olig1^{+/+};Dnmt1^{fl/fl}* and *Olig1^{cre/+};Dnmt1^{fl/fl}* mice, *Olig1^{+/+};Dnmt3a^{fl/fl}* and *Olig1^{cre/+};Dnmt3a^{fl/fl}* mice, and *Cnp^{+/+};Dnmt1^{fl/fl}* and *Cnp^{cre/+};Dnmt1^{fl/fl}* mice stained for MBP (green) and OLIG2 (red). Scale bars, 100 μ m.

(E–G) Gross analysis of P14 *Olig1^{cre/+};Dnmt1^{fl/fl}* mutants revealed minimal differences in body size compared to controls (E) and complete absence of white matter in spinal cord (F) and brain stem (circle in G). Scale bars, 600 μ m (E) and 200 μ m (F and G).

(H) Electron micrograph analysis of P16 spinal cord and corpus callosum sections reveal severe hypomyelination in the *Olig1^{cre/+};Dnmt1^{fl/fl}* mice. Scale bar, 1 μ m. See also Figure S3 and Movie S1.

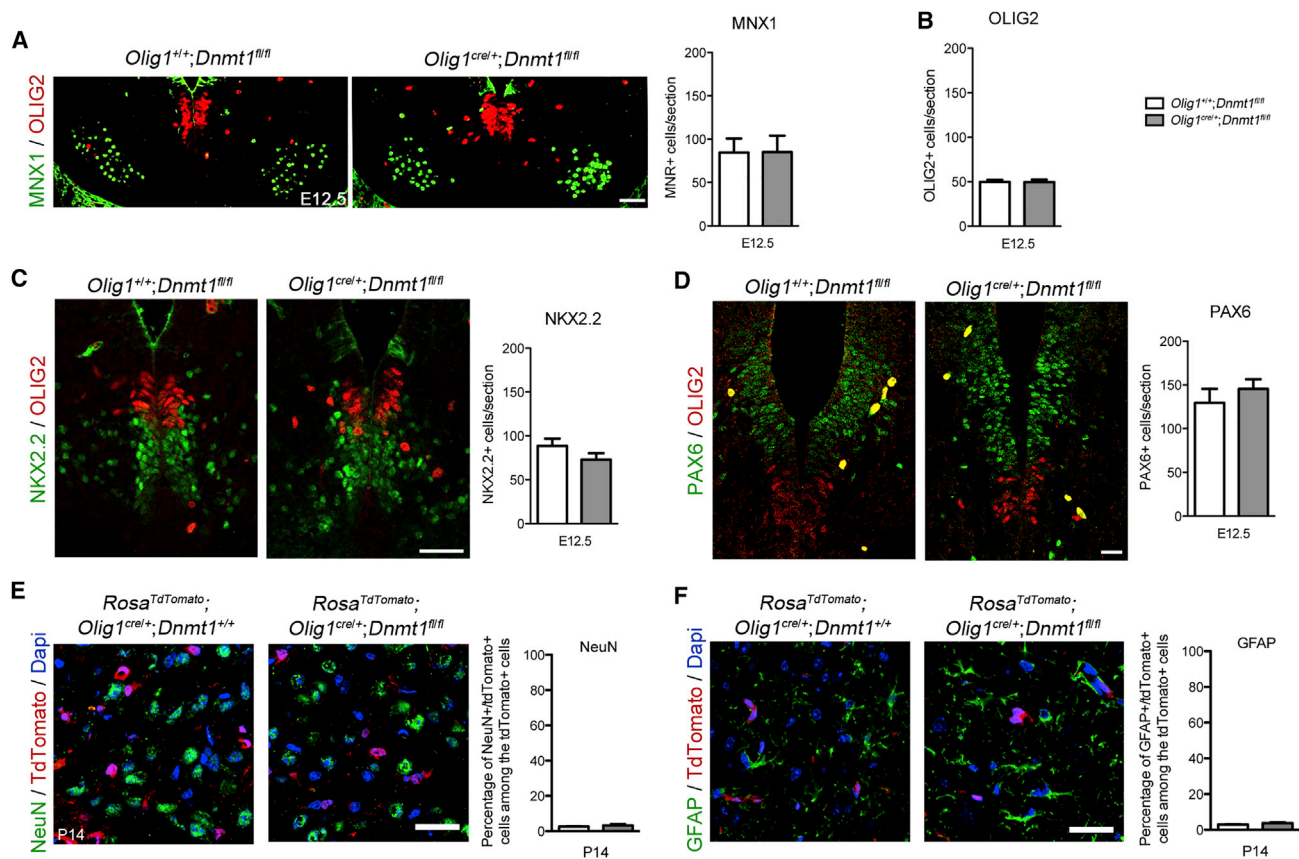


Figure 4. Normal Cell Specification in *Olig1^{cre/+};Dnmt1^{fl/fl}* Spinal Cord**

(A) Representative confocal image of E12.5 spinal cord sections from *Olig1^{+/+};**Dnmt1^{fl/fl}* and *Olig1^{cre/+};**Dnmt1^{fl/fl}* mice, stained for OLIG2 (red) and MNX1 (green), and quantification of MNX1+ cells in control (white bars) and mutants (gray bars).

(B) Quantification of OLIG2+ cells in controls and mutants.

(C) Representative E12.5 spinal cord sections stained for OLIG2 (red) and NKX2.2 (green) and relative quantification in controls and mutants.

(D) Representative E12.5 spinal cord sections stained for OLIG2 (red) and PAX6 (green) and relative quantification in controls and mutants.

(E and F) Representative P14 spinal cord sections from *Rosa^{TdTomato};**Olig1^{cre/+};**Dnmt1^{+/+}* and *Rosa^{TdTomato};**Olig1^{cre/+};**Dnmt1^{fl/fl}* mice, stained for NeuN (E) or GFAP (F), and percentage of NeuN+/TdTomato+ (E) or GFAP+/TdTomato+ (F) cells among the TdTomato+ cells.

Scale bars, 150 μ m. Data indicate mean \pm SEM. * $p < 0.05$ (ANOVA and Student's t test).

did not induce any change (Figure 7H). These results suggested that *Dnmt1* ablation in OPCs resulted in inappropriate protein folding, likely as a result of the dramatic changes in alternative splicing events detected in mutants.

Overall, this study supports a role for DNA methylation in OL differentiation that goes beyond the repression of progenitor stage genes and includes the regulation of alternative splicing events at later stages of differentiation, which are critical for the attainment of the myelinating phenotype.

DISCUSSION

OPCs are the last cells to differentiate in the developing CNS, and their maturation is characterized by the silencing of alternative lineages and genome-wide deposition of repressive histone K9 and K27 methylation marks (Liu et al., 2015; Sher et al., 2008, 2012). Our genome-wide analysis of differentially methylated genes during the differentiation of OPCs into OLs directly sorted

from developing brains revealed hypermethylation at the promoter of OPC-specific genes in response to mitogens (such as *Pdgfra*), as well as regulators of DNA replication (such as *Cdc6*), and neuronal-lineage genes (such as *Pax6*). This suggested that DNA methylation contributes to the transition of OPCs to OLs by regulating cell-cycle exit and, possibly, lineage choice decisions. The concept of fine-tuning of the DNA methylome during mammalian brain development was previously suggested (Kessler et al., 2016; Lister et al., 2013), and we had predicted two potential outcomes to the ablation of *Dnmts* in OPCs: increased OPC proliferation and potential lineage-choice switch. In neural stem cells, *Dnmt1* ablation led to decreased survival and astroglial differentiation (Fan et al., 2001); in astrocytes, it led to precocious differentiation (Fan et al., 2005; He et al., 2005).

Interestingly, none of the predicted outcomes was observed in mice with *Dnmt1* ablation in the OL lineage. Despite the hypomethylation of myelin genes, OPCs did not undergo precocious

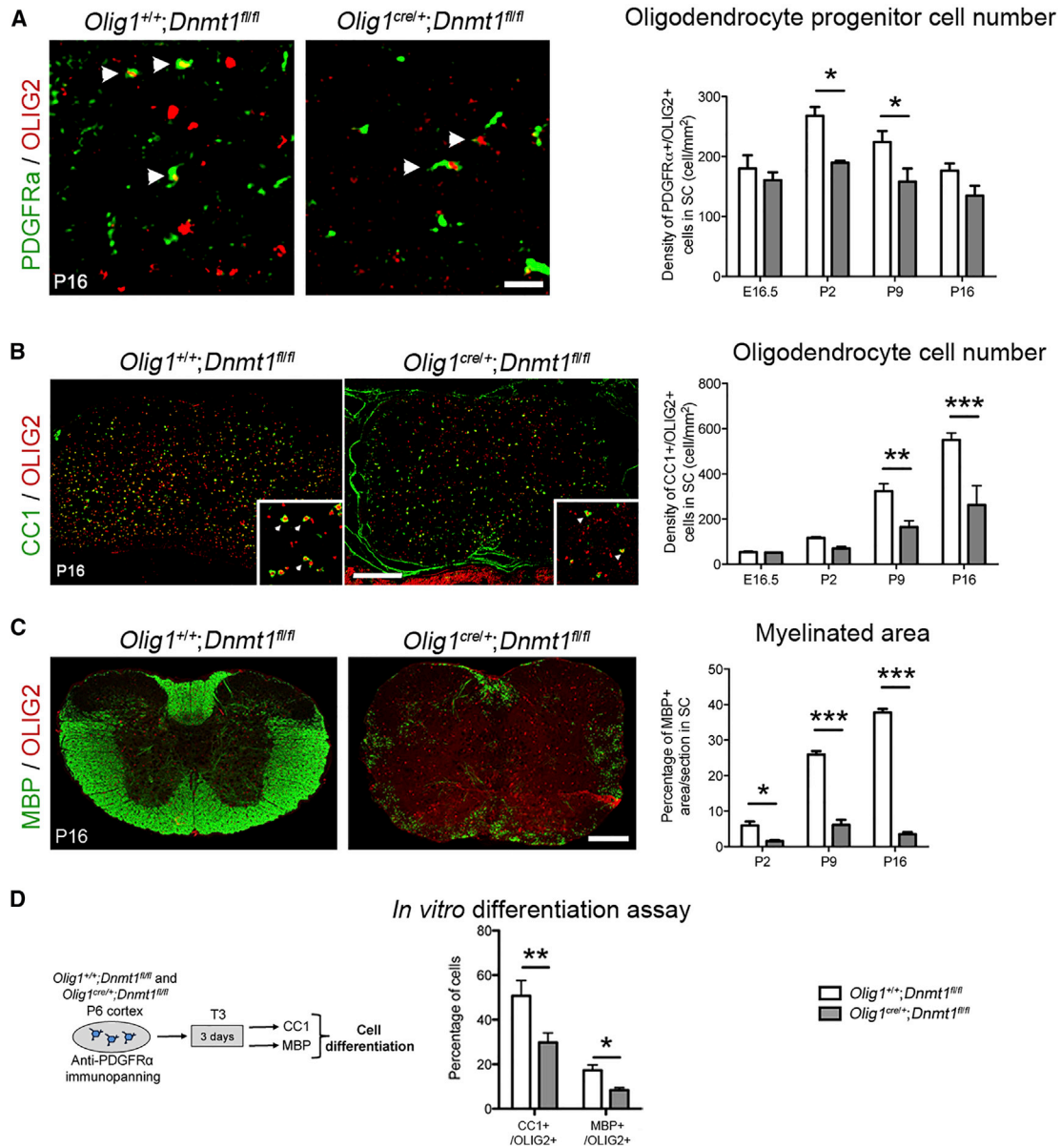


Figure 5. Impaired OPC Cell Differentiation in *Olig1^{cre/+};Dnmt1^{fl/fl}* Mice

(A) Representative P16 spinal cord (SC) sections of *Olig1^{+/+};Dnmt1^{fl/fl}* and *Olig1^{cre/+};Dnmt1^{fl/fl}* mice, stained for OLIG2 (red) and PDGFR α (green), and quantification of PDGFR α +/OLIG2+ cells at indicated time points. Scale bar, 40 μ m.

(B) Representative image of P16 spinal cord sections stained for OLIG2 (red) and CC1 (green) and relative quantification. Scale bar, 100 μ m.

(C) Representative image of P16 spinal cord sections of mutants and controls, stained for OLIG2 (red) and MBP (green) and relative quantification, showing extensive hypo-myelination. Scale bar, 100 μ m.

(D) Schematic of immunopanning from *Olig1^{+/+};Dnmt1^{fl/fl}* and *Olig1^{cre/+};Dnmt1^{fl/fl}* P6 cortex to assess *in vitro* differentiation, and quantification of the number of CC1+ /OLIG2+ and MBP+ /OLIG2+ cells in T3 medium.

Data indicate mean \pm SEM. *p < 0.05; **p < 0.01; ***p < 0.005 (ANOVA).

See also Figure S4.

differentiation. Given the relationship between cell-cycle exit and differentiation (Magri et al., 2014), a potential explanation for the mouse phenotype was the possible retention of OPCs in a proliferative state, which was suggested by the hypomethylation of genes regulating DNA replication (e.g., *Meis2* and *Cdc6*). However, mutant OPCs exited from the cell cycle and inefficiently

differentiated, despite the removal of the “methylation brake” on the promoter of myelin genes. Reduced OPC proliferation was associated with the detection of phosphorylated histone H2AX, a measure of genotoxic stress (Albino et al., 2009; Lawless et al., 2010). This was consistent with the idea that DNMT1 plays a critical role in the fidelity of transmission of

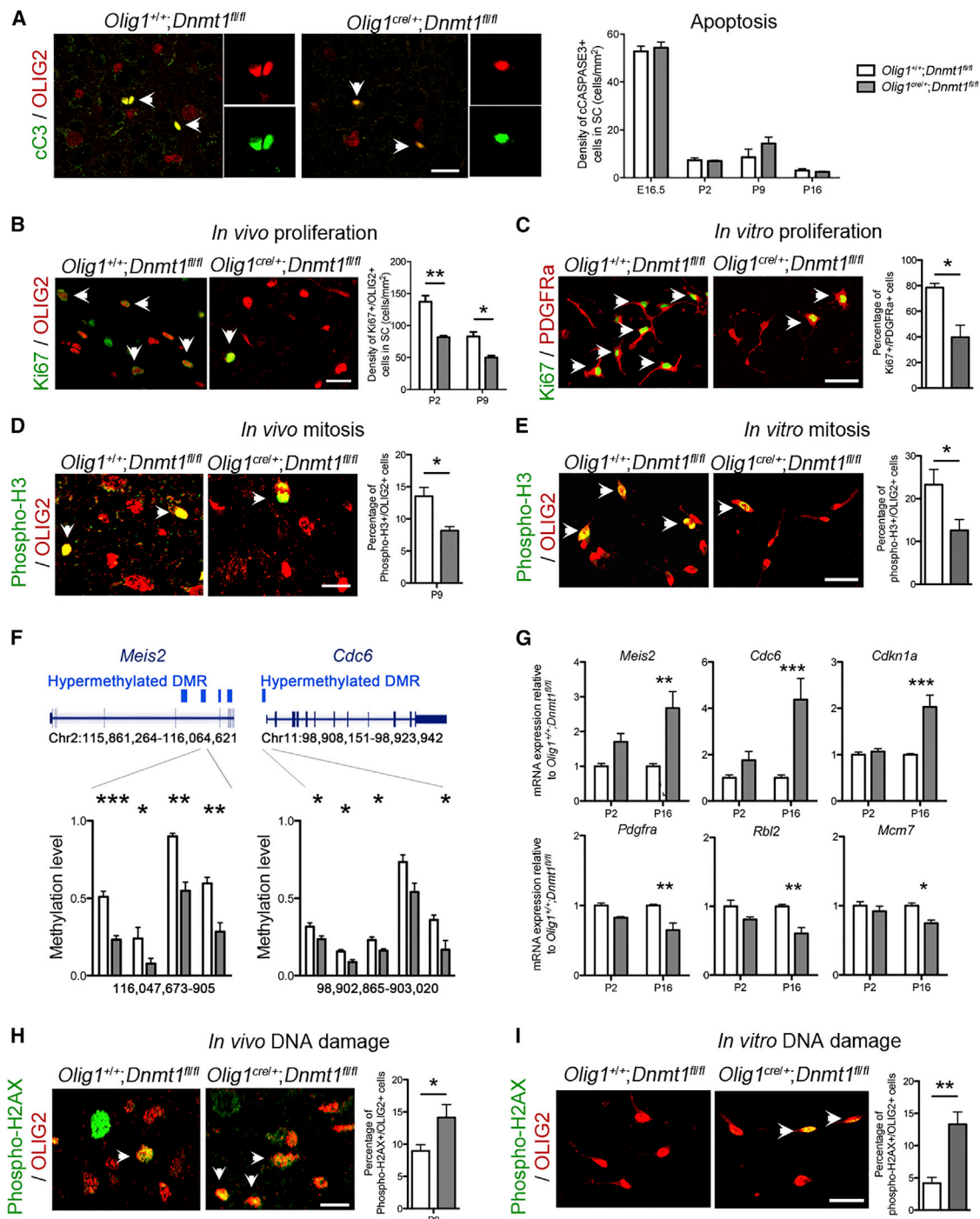


Figure 6. Proliferation Defect and Genotoxic Damage in *Olig1^{cre/+};Dnmt1^{fl/fl}* OPCs

(A) Representative P9 spinal cord sections of *Olig1^{+/+};Dnmt1^{fl/fl}* and *Olig1^{cre/+};Dnmt1^{fl/fl}* mice, stained for OLIG2 (red) and cleaved-CASPASE3 (green), and quantification of cCASPASE3+ cells in the spinal cord at the indicated time points.

(B) Representative P9 spinal cord sections of *Olig1^{+/+};Dnmt1^{fl/fl}* and *Olig1^{cre/+};Dnmt1^{fl/fl}* mice, stained for OLIG2 (red) and Ki67 (green), and quantification of Ki67+/OLIG2+ cells at P2 and P9.

(C) Representative *Olig1^{+/+};Dnmt1^{fl/fl}* and *Olig1^{cre/+};Dnmt1^{fl/fl}* immunopanned OPCs, stained for PDGFR α (red) and Ki67 (green), and quantification of the number of Ki67+/PDGFR α + cells in PDGF + FGF medium.

(D) Representative P9 spinal cord sections of *Olig1^{+/+};Dnmt1^{fl/fl}* and *Olig1^{cre/+};Dnmt1^{fl/fl}* mice, stained for OLIG2 (red) and phospho-H3 (green), and quantification of phospho-H3+/OLIG2+ cells at P9.

(legend continued on next page)

epigenetic information from mother to daughter cells during cell division (Fan et al., 2001; Probst et al., 2009; Sen et al., 2010). In its absence, specific “sensors” induce dsDNA breaks and activate specific kinases that, in turn, phosphorylate the nucleosomal histones and mark these regions as “damaged” (Altaf et al., 2007; Méndez-Acuña et al., 2010; Rossetto et al., 2012). This initiates a response resulting in growth arrest or apoptosis, in an attempt to contain the number of cells with aberrant information (Milutinovic et al., 2003; Unterberger et al., 2006). In contrast to other cell types (Fan et al., 2001; Jacob et al., 2015), OPCs lacking *Dnmt1* did not display massive apoptosis, and we reasoned that this was likely due to the fact that OPCs are the last cells to differentiate at the tail end of development, when all the other organs and systems are already in place, and altered DNA methylation in these cells may not represent an immediate threat to the overall health of the organism.

After exiting from the cell cycle, OPCs only inefficiently differentiated into OLs and they were unable to generate large amounts of myelin components, thereby resulting in a severely hypomyelinated phenotype, which could not be explained simply in terms of cell number reduction. We also did not detect increased expression of neuronal or astrocytic genes, indicative of a potential lineage switch. This was consistent with the results of fate-mapping experiments and highlighted the reliance of lineage choices on multiple modalities of repression requiring the concerted cooperation of DNA methylation and repressive histone methylation marks occurring during OL differentiation (Liu et al., 2015).

At the ultrastructural level, the preservation of axonal diameter in mutants, despite the absence of myelin suggested, at least in part, the preservation of signaling between OLs and axons. However, the detection of enlarged ER cisternae and electron-dense inclusion bodies in mutant OLs was reminiscent of proteinaceous aggregates reported in other cell types (Ronconi et al., 2010; Valetti et al., 1991) and suggested the activation of an ER stress response. A detailed molecular analysis of the three ER response pathways identified the sequential activation of the ATF6 and PERK pathways prior to the engagement of the IRE1 response (Hetz et al., 2013; Osowski and Urano, 2011), validating the results of the ultrastructural data. A potential explanation for the activation of the ER stress response in oligodendroglial cells lacking *Dnmt1* was suggested by RNA sequencing analysis that revealed a massive alteration of alternative splicing. Our analysis identified defective exon-skipping and intron-retention events in mutant cells, while other modalities of splicing, including alternative exons and 5' or 3' acceptor

sites were not affected. It has been previously reported that differential methylation of CpGs in specific genomic areas results in defective splicing (Gelfman et al., 2013; Hnilicová and Staněk, 2011; Iannone and Valcárcel, 2013), and our study provides an in vivo validation, in the CNS, for this proposed model. We validated the co-occurrence of differential DNA methylation and altered retained-intron splicing in selected genes, supporting the concept that DNA methylation is tightly linked to this form of splicing events, and its absence results in a wide rearrangement of RNA-splicing events, which, in turn, may cause aberrant protein folding, possibly leading to the activation of an ER stress response.

We conclude that the role of DNMT1 in OL-lineage cells is more complex than originally anticipated and encompasses the regulation of the proliferative state of OPC, as well as a tight coordination between alternative splicing and protein synthesis in the generation of myelinating OLs.

EXPERIMENTAL PROCEDURES

Animals

All experiments were conducted according to the Icahn School of Medicine at Mount Sinai institutional animal care and use committee (IACUC)-approved protocols. *Dnmt1^{fl/fl}* (Fan et al., 2001; Jackson-Grusby et al., 2001) and *Dnmt3a^{fl/fl}* (Kaneda et al., 2004) mice on a C57BL/6 background were crossed with *Olig1-cre* (Jackson Laboratory), *Cnp-cre* mice (Lappe-Siefke et al., 2003), or *Rosa26-loxP-STOP-loxP-TdTomato* mice (Jackson Laboratory).

Cell Sorting

OPCs were isolated from P2 *Pdgfra-GFP*, P5 *Olig1^{cre/+};Dnmt1^{fl/fl};Pdgfra-GFP* or *Olig1^{+/+};Dnmt1^{fl/fl};Pdgfra-GFP* brains (Klinghoffer et al., 2002) and OLs from P18 *Plp1-GFP* brains (Spassky et al., 1998) using FACS as described previously (Moyon et al., 2015).

DNA Methylation Analysis

ERRBS libraries were prepared from 50 ng input DNA per biological replicate following a modified (Akalın et al., 2012) protocol (Gu et al., 2011) and sequenced using the Illumina HiSeq 2000 instrument. DMRs were selected at a *q* value <0.05 and with a minimum mean difference of 10% per region. DMRs were independently validated using MassARRAY EpiTYPER assays (Sequenom), as previously described (Huynh et al., 2014). Genomic DNA was sodium bisulfite treated using an EpiTect Bisulfite Kit (QIAGEN). See details and primers in the Supplemental Information.

Gene Expression Analysis

Approximately 250 ng of total RNA per sample was used for library construction with the TruSeq RNA Sample Prep Kit (Illumina) and sequenced using the Illumina HiSeq 2000 and the Illumina HiSeq 2500 instruments according to the manufacturer's instructions for 50-bp (OPC-OL) or 100-bp (*Dnmt1cKO*) paired-end read runs. High-quality reads were aligned to the mouse reference

(E) Representative *Olig1^{+/+};Dnmt1^{fl/fl}* and *Olig1^{cre/+};Dnmt1^{fl/fl}* immunopanned OPCs, stained for OLIG2 (red) and phospho-H3 (green), and quantification of the number of phospho-H3+/OLIG2+ cells in PDGF + FGF medium. White arrowheads indicate double-positive cells.

(F) Methylation of individual CpGs assessed by MassARRAY EpiTYPER of *Meis2* and *Cdc6* revealed hypomethylation. In blue is the complete gene structure, including hypermethylated DMRs observed in differentiating OLs (blue rectangles). Dotted lines identify the zoomed region containing the DMRs. Methylation levels of indicated CpGs is shown for control (white) and mutant (gray) sorted OPCs.

(G) Real-time qPCR analysis of transcript levels of the indicated genes in P2 and P16 spinal cord of *Olig1^{cre/+};Dnmt1^{fl/fl}* mice (gray) relative to the levels in controls (white).

(H) Representative P9 spinal cord sections of *Olig1^{+/+};Dnmt1^{fl/fl}* and *Olig1^{cre/+};Dnmt1^{fl/fl}* mice, stained for OLIG2 (red) and the genotoxic stress marker phospho-H2AX (green), with relative quantification.

(I) Representative *Olig1^{+/+};Dnmt1^{fl/fl}* and *Olig1^{cre/+};Dnmt1^{fl/fl}* immunopanned OPCs, stained for OLIG2 (red) and phospho-H2AX (green), and relative quantification in proliferating OPCs.

Scale bars, 25 μ m. Data indicate mean \pm SEM. **p* < 0.05; ***p* < 0.01; ****p* < 0.005 (ANOVA and Student's *t* test).

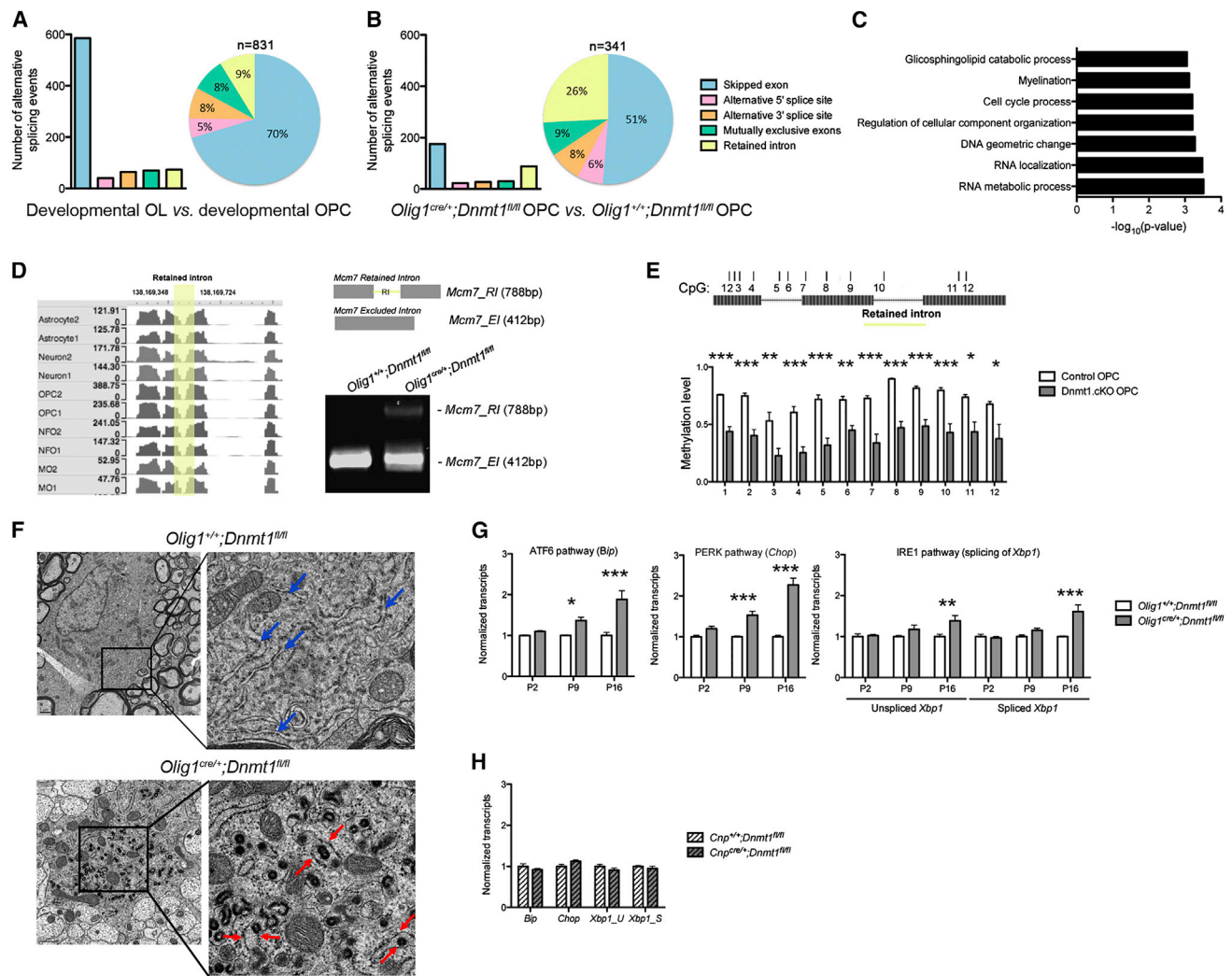


Figure 7. Ablation of *Dnmt1* in OPCs Results in Aberrant Alternative Splicing Events and ER Stress

(A) Histogram and pie chart showing, respectively, number and proportion of alternative splicing events during normal OL development (classified in five categories).

(B) Histogram and pie chart showing, respectively, number and proportion of alternative splicing events in mutant OPCs compared to controls.

(C) GO of genes alternatively spliced in mutant *Olig1^{cre/+};Dnmt1^{fl/fl}* OPCs compared to *Olig1^{+/+};Dnmt1^{fl/fl}* OPCs.

(D) Validation of retained-intron splicing of *Mcm7* in *Olig1^{cre/+};Dnmt1^{fl/fl}* OPCs by PCR.

(E) Methylation differences in individual CpGs between control (white) and mutant (gray) DNA isolated from OPC and assessed by MassARRAY EpiTYPER.

(F) Ultrastructural analysis identifies a dilated ER with inclusions (red arrows) in *Olig1^{cre/+};Dnmt1^{fl/fl}* mice, compared to *Olig1^{+/+};Dnmt1^{fl/fl}* controls (blue arrows).

(G) Real-time qPCR analysis of genes involved in ER stress response, including the ATF6, PERK, and IRE1 pathways, analyzed in P2, P9, and P16 spinal cord of controls (*Olig1^{+/+};Dnmt1^{fl/fl}*) and mutants (*Olig1^{cre/+};Dnmt1^{fl/fl}*).

(H) Real-time qPCR analysis of ER stress response target genes assessed in P9 spinal cord of *Cnp^{+/+};Dnmt1^{fl/fl}* and *Cnp^{cre/+};Dnmt1^{fl/fl}* mice.

Data indicate mean \pm SEM. *p < 0.05; **p < 0.01; ***p < 0.005 (ANOVA). See also Figure S5.

genome (mm10), RefSeq exons, splicing junctions, and contamination databases (ribosome and mitochondria sequences) using the Burrows-Wheeler Aligner (BWA) algorithm. The read count for each RefSeq transcript was extracted using uniquely aligned reads to exon and splice-junction regions. The raw read counts were input into DESeq2 v1.2.5 (Anders and Huber, 2010) to normalize the signal for each transcript and to ascertain differential gene expression with associated q values. Differentially expressed genes were selected at a p value < 0.05 and q value < 0.01 with a fold change > 2 for the OPC-OL comparison only. To identify enriched gene functions, we computed hypergeometric p values for over-representation of each biological

process GO category using GOrilla (Eden et al., 2009). For genome-wide annotation, org.Mm.eg.db was used in the GOstats R package (Falcon and Gentleman, 2007).

To identify alternative splicing, we used a published Bayesian statistical framework on RNA-seq data from either *Pdgfr α -GFP* and *Plp1-GFP* sorted cells or *Olig1^{cre/+};Dnmt1^{fl/fl};Pdgfr α -GFP* and *Olig1^{+/+};Dnmt1^{fl/fl};Pdgfr α -GFP* sorted cells (Shen et al., 2012). MATS can automatically detect and analyze alternative splicing events corresponding to all major types of alternative splicing patterns, including the following: skipped exon (SE), alternative 5' splicing site (A5SS), alternative 3' splicing site (A3SS), mutually exclusive

exon (MXE), and retained intron (RI). Spliced events between two conditions were defined by a *p* value <0.05. Additional details are given in the [Supplemental Information](#).

Electron Microscopy and Immunohistochemistry

For electron microscopy, mice were deeply anesthetized and transcardially perfused with 0.9% NaCl, followed by 0.1 M Millonig's solution containing 4% paraformaldehyde and 5% glutaraldehyde (pH 7.3), followed by 2 weeks of post-fixation in the same fixative solution at 4°C, as previously described (He et al., 2007). For immunohistochemistry, animals were perfused with 4% paraformaldehyde and post-fixed overnight in the same solution at 4°C. Tissue samples were then transferred to 70% ethanol, sequentially dehydrated, and embedded in paraffin. Immunohistochemistry was performed in 4- to 10- μ m sections. All images were acquired using a Zeiss Observer A1 fluorescent microscope or a Zeiss LSM780 upright confocal microscope. Quantification was carried out using ImageJ on two to three sections per mouse and three to four mice for each age and genotype.

Primary OPC Cultures

Mouse OPCs were isolated from P7 mice as described previously (Cahoy et al., 2008), plated in 24-well dishes and kept proliferating in platelet-derived growth factor (PDGF)-AA (10 ng/ml) and basic fibroblast growth factor (bFGF) (20 ng/ml) or differentiated with T3 hormone (45 nM).

Rat primary glial cells were generated from 2- to 3-day-old Sprague-Dawley rats (Harlan UK), according to published procedures.

Statistical Methods

A minimum of three replicates per group was used for each experiment. Unpaired Student's *t* test was used for cell counts and transcript levels for every two datasets following a normal distribution. A two-way ANOVA was used to compare three or more sets of data, including cell counts and MassARRAY data. For all graphs, error bars indicate mean \pm SEM.

ACCESSION NUMBERS

The accession number for sequencing data reported in this paper is GEO: GSE66047.

SUPPLEMENTAL INFORMATION

Supplemental Information includes Supplemental Experimental Procedures, five figures, five tables, and one movie and can be found with this article online at <http://dx.doi.org/10.1016/j.celrep.2016.03.060>.

AUTHOR CONTRIBUTIONS

S.M. and J.L.H. generated and characterized the conditional knockout mice, performed the RT-qPCR, and analyzed RNA-seq and ERBSS data; S.M., R.L., and D.D. performed the lineage immunohistochemistry; S.M. alone performed FACS, EpiTYPER MassARRAY, and immunocytochemistry; J.L.D. performed the EM experiments; F.Z. performed the alternative splicing analysis; G.F. provided the *fox* mice; D.M. performed 5-mC reactivity experiments; S.M., J.L.H., D.M., S.Y., C.L., R.J.M.F., G.R.J., B.E., J.Z., M.W., and P.C. analyzed the data and provided comments; S.M. and P.C. wrote and revised the manuscript.

ACKNOWLEDGMENTS

Thanks to A. Alonso, Y. Li, X. Zhang, Y. Xin, and the Flow Cytometry Core CyPS (Pitie-Salpetriere Hospital, Paris) for experimental support. Thanks to Drs. A. Sharp, C. Watson, J. Feng, and L. Wrabetz for insightful discussions and Dr. J. Svaren for comments on the manuscript. This work was supported by NIH-NINDS grants R37NS042925 and NS-R0152738 (P.C.) and F31NS077504 (J.L.H.), the UK Multiple Sclerosis Society (R.J.M.F.), and NIH-NIMH grant R01MH090948 (J.Z.).

Received: March 26, 2015

Revised: February 8, 2016

Accepted: March 15, 2016

Published: April 14, 2016

REFERENCES

- Akalin, A., Garrett-Bakelman, F.E., Kormaksson, M., Busuttill, J., Zhang, L., Khrebtukova, I., Milne, T.A., Huang, Y., Biswas, D., Hess, J.L., et al. (2012). Base-pair resolution DNA methylation sequencing reveals profoundly divergent epigenetic landscapes in acute myeloid leukemia. *PLoS Genet.* **8**, e1002781.
- Albino, A.P., Jorgensen, E.D., Rainey, P., Gillman, G., Clark, T.J., Gietl, D., Zhao, H., Traganos, F., and Darzynkiewicz, Z. (2009). gammaH2AX: A potential DNA damage response biomarker for assessing toxicological risk of tobacco products. *Mutat. Res.* **678**, 43–52.
- Altaf, M., Saksouk, N., and Côté, J. (2007). Histone modifications in response to DNA damage. *Mutat. Res.* **678**, 81–90.
- Anders, S., and Huber, W. (2010). Differential expression analysis for sequence count data. *Genome Biol.* **11**, R106.
- Cahoy, J.D., Emery, B., Kaushal, A., Foo, L.C., Zamanian, J.L., Christopherson, K.S., Xing, Y., Lubischer, J.L., Krieg, P.A., Krupenko, S.A., et al. (2008). A transcriptome database for astrocytes, neurons, and oligodendrocytes: a new resource for understanding brain development and function. *J. Neurosci.* **28**, 264–278.
- Eden, E., Navon, R., Steinfeld, I., Lipson, D., and Yakhini, Z. (2009). GOrilla: a tool for discovery and visualization of enriched GO terms in ranked gene lists. *BMC Bioinformatics* **10**, 48.
- Falcon, S., and Gentleman, R. (2007). Using GOstats to test gene lists for GO term association. *Bioinformatics* **23**, 257–258.
- Fan, G., Beard, C., Chen, R.Z., Csankovszki, G., Sun, Y., Siniia, M., Biniszkievicz, D., Bates, B., Lee, P.P., Kuhn, R., et al. (2001). DNA hypomethylation perturbs the function and survival of CNS neurons in postnatal animals. *J. Neurosci.* **21**, 788–797.
- Fan, G., Martinowich, K., Chin, M.H., He, F., Fouse, S.D., Hutnick, L., Hattori, D., Ge, W., Shen, Y., Wu, H., et al. (2005). DNA methylation controls the timing of astroglialogenesis through regulation of JAK-STAT signaling. *Development* **132**, 3345–3356.
- Gelfman, S., Cohen, N., Yearim, A., and Ast, G. (2013). DNA-methylation effect on cotranscriptional splicing is dependent on GC architecture of the exon-intron structure. *Genome Res.* **23**, 789–799.
- Gu, H., Smith, Z.D., Bock, C., Boyle, P., Gnirke, A., and Meissner, A. (2011). Preparation of reduced representation bisulfite sequencing libraries for genome-scale DNA methylation profiling. *Nat. Protoc.* **6**, 468–481.
- He, F., Ge, W., Martinowich, K., Becker-Catania, S., Coskun, V., Zhu, W., Wu, H., Castro, D., Guillemot, F., Fan, G., et al. (2005). A positive autoregulatory loop of Jak-STAT signaling controls the onset of astroglialogenesis. *Nat. Neurosci.* **8**, 616–625.
- He, Y., Dupree, J., Wang, J., Sandoval, J., Li, J., Liu, H., Shi, Y., Nave, K.A., and Casaccia-Bonnel, P. (2007). The transcription factor Yin Yang 1 is essential for oligodendrocyte progenitor differentiation. *Neuron* **55**, 217–230.
- Hetz, C., Chevet, E., and Harding, H.P. (2013). Targeting the unfolded protein response in disease. *Nat. Rev. Drug Discov.* **12**, 703–719.
- Hnilicová, J., and Staněk, D. (2011). Where splicing joins chromatin. *Nucleus* **2**, 182–188.
- Hutnick, L.K., Golshani, P., Namihira, M., Xue, Z., Matynia, A., Yang, X.W., Silva, A.J., Schweizer, F.E., and Fan, G. (2009). DNA hypomethylation restricted to the murine forebrain induces cortical degeneration and impairs postnatal neuronal maturation. *Hum. Mol. Genet.* **18**, 2875–2888.
- Huynh, J.L., Garg, P., Thin, T.H., Yoo, S., Dutta, R., Trapp, B.D., Haroutunian, V., Zhu, J., Donovan, M.J., Sharp, A.J., and Casaccia, P. (2014). Epigenome-wide differences in pathology-free regions of multiple sclerosis-affected brains. *Nat. Neurosci.* **17**, 121–130.

- Iannone, C., and Valcárcel, J. (2013). Chromatin's thread to alternative splicing regulation. *Chromosoma* 122, 465–474.
- Jackson-Grusby, L., Beard, C., Possemato, R., Tudor, M., Fambrough, D., Csankovszki, G., Dausman, J., Lee, P., Wilson, C., Lander, E., and Jaenisch, R. (2001). Loss of genomic methylation causes p53-dependent apoptosis and epigenetic deregulation. *Nat. Genet.* 27, 31–39.
- Jacob, V., Chernyavskaya, Y., Chen, X., Tan, P.S., Kent, B., Hoshida, Y., and Sadler, K.C. (2015). DNA hypomethylation induces a DNA replication-associated cell cycle arrest to block hepatic outgrowth in *uhrf1* mutant zebrafish embryos. *Development* 142, 510–521.
- Kaneda, M., Okano, M., Hata, K., Sado, T., Tsujimoto, N., Li, E., and Sasaki, H. (2004). Essential role for de novo DNA methyltransferase *Dnmt3a* in paternal and maternal imprinting. *Nature* 429, 900–903.
- Kessler, N.J., Van Baak, T.E., Baker, M.S., Laritsky, E., Coarfa, C., and Waterland, R.A. (2016). CpG methylation differences between neurons and glia are highly conserved from mouse to human. *Hum. Mol. Genet.* 25, 223–232.
- Kevelam, S.H., Taube, J.R., van Spaendonk, R.M.L., Bertini, E., Sperle, K., Tamopolsky, M., Tonduti, D., Valente, E.M., Travaglini, L., Siermans, E.A., et al. (2015). Altered PLP1 splicing causes hypomyelination of early myelinating structures. *Ann. Clin. Transl. Neurol.* 2, 648–661.
- Klinghoffer, R.A., Hamilton, T.G., Hoch, R., and Soriano, P. (2002). An allelic series at the *PDGFalphaR* locus indicates unequal contributions of distinct signaling pathways during development. *Dev. Cell* 2, 103–113.
- Lappe-Siefke, C., Goebbels, S., Gravel, M., Nicksch, E., Lee, J., Braun, P.E., Griffiths, I.R., and Nave, K.A. (2003). Disruption of *Cnp1* uncouples oligodendroglial functions in axonal support and myelination. *Nat. Genet.* 33, 366–374.
- Lawless, C., Wang, C., Jurk, D., Merz, A., Zglinicki, T., and Passos, J.F. (2010). Quantitative assessment of markers for cell senescence. *Exp. Gerontol.* 45, 772–778.
- Li, E., Bestor, T.H., and Jaenisch, R. (1992). Targeted mutation of the DNA methyltransferase gene results in embryonic lethality. *Cell* 69, 915–926.
- Lister, R., Mukamel, E.A., Nery, J.R., Urich, M., Puddifoot, C.A., Johnson, N.D., Lucero, J., Huang, Y., Dwork, A.J., Schultz, M.D., et al. (2013). Global epigenomic reconfiguration during mammalian brain development. *Science* 341, 1237905.
- Liu, J., Magri, L., Zhang, F., Marsh, N.O., Albrecht, S., Huynh, J.L., Kaur, J., Kuhlmann, T., Zhang, W., Slesinger, P.A., and Casaccia, P. (2015). Chromatin landscape defined by repressive histone methylation during oligodendrocyte differentiation. *J. Neurosci.* 35, 352–365.
- Magri, L., Swiss, V.A., Jablonska, B., Lei, L., Pedre, X., Walsh, M., Zhang, W., Gallo, V., Canoll, P., and Casaccia, P. (2014). *E2F1* coregulates cell cycle genes and chromatin components during the transition of oligodendrocyte progenitors from proliferation to differentiation. *J. Neurosci.* 34, 1481–1493.
- Méndez-Acuña, L., Di Tomaso, M.V., Palitti, F., and Martínez-López, W. (2010). Histone post-translational modifications in DNA damage response. *Cytogenet. Genome Res.* 128, 28–36.
- Milutinovic, S., Zhuang, Q., Niveleau, A., and Szyf, M. (2003). Epigenomic stress response. Knockdown of DNA methyltransferase 1 triggers an intra-S-phase arrest of DNA replication and induction of stress response genes. *J. Biol. Chem.* 278, 14985–14995.
- Moyon, S., Dubessy, A.L., Aigrot, M.S., Trotter, M., Huang, J.K., Dauphinot, L., Potier, M.C., Kerninon, C., Melik Parsadaniantz, S., Franklin, R.J.M., and Lubetzki, C. (2015). Demyelination causes adult CNS progenitors to revert to an immature state and express immune cues that support their migration. *J. Neurosci.* 35, 4–20.
- Nave, K.A., Lai, C., Bloom, F.E., and Milner, R.J. (1987). Splice site selection in the proteolipid protein (PLP) gene transcript and primary structure of the DM-20 protein of central nervous system myelin. *Proc. Natl. Acad. Sci. USA* 84, 5665–5669.
- Ono, T., Uehara, Y., Kurishita, A., Tawa, R., and Sakurai, H. (1993). Biological significance of DNA methylation in the ageing process. *Age Ageing* 22, S34–S43.
- Osowski, C.M., and Urano, F. (2011). Measuring ER stress and the unfolded protein response using mammalian tissue culture system. *Methods Enzymol.* 490, 71–92.
- Probst, A.V., Dunleavy, E., and Almouzni, G. (2009). Epigenetic inheritance during the cell cycle. *Nat. Rev. Mol. Cell Biol.* 10, 192–206.
- Ronzoni, R., Anelli, T., Brunati, M., Cortini, M., Fagioli, C., and Sitia, R. (2010). Pathogenesis of ER storage disorders: modulating Russell body biogenesis by altering proximal and distal quality control. *Traffic* 11, 947–957.
- Rossetto, D., Avvakumov, N., and Côté, J. (2012). Histone phosphorylation: a chromatin modification involved in diverse nuclear events. *Epigenetics* 7, 1098–1108.
- Sen, G.L., Reuter, J.A., Webster, D.E., Zhu, L., and Khavari, P.A. (2010). DNMT1 maintains progenitor function in self-renewing somatic tissue. *Nature* 463, 563–567.
- Shen, S., Park, J.W., Huang, J., Dittmar, K.A., Lu, Z.X., Zhou, Q., Carstens, R.P., and Xing, Y. (2012). MATS: a Bayesian framework for flexible detection of differential alternative splicing from RNA-Seq data. *Nucleic Acids Res.* 40, e61.
- Sher, F., Rössler, R., Brouwer, N., Balasubramaniyan, V., Boddeke, E., and Copray, S. (2008). Differentiation of neural stem cells into oligodendrocytes: involvement of the polycomb group protein *Ezh2*. *Stem Cells* 26, 2875–2883.
- Sher, F., Boddeke, E., Olah, M., and Copray, S. (2012). Dynamic changes in *Ezh2* gene occupancy underlie its involvement in neural stem cell self-renewal and differentiation towards oligodendrocytes. *PLoS ONE* 7, e40399.
- Smith, Z.D., and Meissner, A. (2013). DNA methylation: roles in mammalian development. *Nat. Rev. Genet.* 14, 204–220.
- Spassky, N., Goujet-Zalc, C., Parmantier, E., Olivier, C., Martinez, S., Ivanova, A., Ikenaka, K., Macklin, W., Cerruti, I., Zalc, B., and Thomas, J.L. (1998). Multiple restricted origin of oligodendrocytes. *J. Neurosci.* 18, 8331–8343.
- Takizawa, T., Nakashima, K., Namihira, M., Ochiai, W., Uemura, A., Yanagisawa, M., Fujita, N., Nakao, M., and Taga, T. (2001). DNA methylation is a critical cell-intrinsic determinant of astrocyte differentiation in the fetal brain. *Dev. Cell* 1, 749–758.
- Tawa, R., Ono, T., Kurishita, A., Okada, S., and Hirose, S. (1990). Changes of DNA methylation level during pre- and postnatal periods in mice. *Differentiation* 45, 44–48.
- Unterberger, A., Andrews, S.D., Weaver, I.C., and Szyf, M. (2006). DNA methyltransferase 1 knockdown activates a replication stress checkpoint. *Mol. Cell Biol.* 26, 7575–7586.
- Valetti, C., Grossi, C.E., Milstein, C., and Sitia, R. (1991). Russell bodies: a general response of secretory cells to synthesis of a mutant immunoglobulin which can neither exit from, nor be degraded in, the endoplasmic reticulum. *J. Cell Biol.* 115, 983–994.
- Varela-Rey, M., Iruarizaga-Lejarreta, M., Lozano, J.J., Aransay, A.M., Fernandez, A.F., Lavin, J.L., Mosen-Ansorena, D., Berdasco, M., Turmaine, M., Luka, Z., et al. (2014). S-adenosylmethionine levels regulate the schwann cell DNA methylome. *Neuron* 81, 1024–1039.
- Yearim, A., Gelfman, S., Shayevitch, R., Melcer, S., Glaich, O., Mallm, J.-P., Nissim-Rafinia, M., Cohen, A.-H.S., Rippe, K., Meshorer, E., and Ast, G. (2015). HP1 is involved in regulating the global impact of DNA methylation on alternative splicing. *Cell Rep.* 10, 1122–1134.
- Yura, K., Shionyu, M., Hagino, K., Hijikata, A., Hirashima, Y., Nakahara, T., Eguchi, T., Shinoda, K., Yamaguchi, A., Takahashi, K., et al. (2006). Alternative splicing in human transcriptome: functional and structural influence on proteins. *Gene* 380, 63–71.
- Zhang, Y., Chen, K., Sloan, S.A., Bennett, M.L., Scholze, A.R., O'Keefe, S., Phatnani, H.P., Guarnieri, P., Caneda, C., Ruderisch, N., et al. (2014). An RNA-sequencing transcriptome and splicing database of glia, neurons, and vascular cells of the cerebral cortex. *J. Neurosci.* 34, 11929–11947.
- Zhou, Q., and Anderson, D.J. (2002). The bHLH transcription factors OLIG2 and OLIG1 couple neuronal and glial subtype specification. *Cell* 109, 61–73.